Assessment of Human Corneas Prior to Transplantation Using High-Resolution Two-Photon Imaging

Ana Batista,[1,2] Hans Georg Breunig,[2] Aisada König,[1,2] Andreas Schindele,[2] Tobias Hager,[3] Berthold Seitz,[3,4] António Miguel Morgado,[5,6] and Karsten König[1,2]

[1]Saarland University, Biophotonics and Laser Technology, Saarbruecken, Germany
[2]JenLab GmbH, Jena, Germany
[3]Department of Ophthalmology, Medical Center, Saarland University, Homburg/Saar, Germany
[4]Lions Cornea Bank Saar-Lor-Lux, Trier/Westpfalz, Medical Center, Homburg/Saar, Germany
[5]Institute for Biomedical Imaging and Life Sciences, University of Coimbra, Azinhaga Santa Comba-Celas, Coimbra, Portugal
[6]Department of Physics, University of Coimbra, Coimbra, Portugal

Correspondence: Karsten König, Saarland University, Biophotonics and Laser Technology, Campus A5.1, Saarbruecken 66123, Germany; k.koenig@blt.uni-saarland.de.

Submitted: April 6, 2017
Accepted: November 30, 2017

Citation: Batista A, Breunig HG, König A, et al. Assessment of human corneas prior to transplantation using high-resolution two-photon imaging. *Invest Ophthalmol Vis Sci*. 2018;59:176–184. https://doi.org/10.1167/iovs.17-22002

Purpose. The purpose of this study was to evaluate the feasibility of using two-photon imaging (TPI) to assess the condition of human corneas for transplantation.

Methods. Human corneas were imaged after different storage times: short-term (STS), medium-term (MTS), and long-term (LTS) storage. A high-resolution, custom-built 5-dimensional multiphoton microscope with 12-fs pulsed laser excitation was used for image acquisition.

Results. Optical discrimination between different corneal layers and sublayers based on their morphologic characteristics revealed by two-photon autofluorescence (AF) is possible. Furthermore, all layers were characterized based on AF lifetimes to gain information on metabolic activities of cells. The NAD(P)H free to protein-bound ratio (a_1/a_2) of epithelial cells increased significantly in both MTS and LTS corneas compared with STS corneas. In endothelial cells, NAD(P)H a_1/a_2 was significantly increased in MTS samples. For keratocytes, the NAD(P)H a_1/a_2 decreased significantly with storage time. This could indicate that the metabolic activity of the epithelial and endothelial cells reduces, whereas the activity of keratocytes increases with storage time. The analysis of the stroma SHG images indicated that the organization of collagen fibers decreases with storage time. The feasibility of measuring the endothelial cell density (ECD) using TPI was demonstrated. An ECD of 1461 $\pm$ 190 cells/mm^2 was obtained for MTS samples based on TPI.

Conclusions. TPI can provide information not accessible by current clinical methods, such as the cells' metabolic state and structural organization of the stroma, with subcellular resolution. Thus, it may improve the screening process of corneas prior to transplantation and might help to optimize the storage conditions.

Keywords: two-photon imaging, optical metabolic imaging, second-harmonic generation, femtosecond lasers, fluorescence lifetime imaging

Corneal pathologies and dystrophies can ultimately lead to blindness. In fact, they are the second major cause of blindness worldwide.[1] When other treatments fail, the patients' vision can only be restored through corneal transplantation. Corneal transplants were performed successfully for the first time in the early 20th century,[2] and, nowadays, are the most common type of transplants in the world.[3] However, the worldwide demand for corneas tremendously exceeds the supply (only 1 cornea is available for each 70 needed).[3] Meanwhile, a large amount of the donated samples are classified as being unsuitable for transplantation.[3] The reasons why cornea samples may be excluded include positive blood serology and the donors' medical record. However, the largest percentage of samples is excluded due to problems regarding tissue suitability, such as a low endothelium cell density (ECD).[4,5] By improving the method for classification of corneas as being suitable or unsuitable for transplantation, the donated corneas could be used more efficiently. The current imaging modalities used to assess tissue suitability only provide information on corneal anatomy and morphology. As such, the corneal cell metabolism and the structural organization of stroma are disregarded. In this work, we study the feasibility of using two-photon imaging (TPI) to evaluate the suitability of donor corneas for transplantation through the analysis of the cells' metabolism and stroma architecture.

TPI is already an important method for noninvasive, label-free, high-resolution imaging of biological samples. Because excitation is limited to the tiny focal volume, TPI inherently provides optical sectioning, making possible three-dimensional (3D) characterization of the tissue.[6] Further well-known advantages include lower photo-damage and -bleaching compared with one-photon fluorescence microscopy.[6,7]

The cells' metabolic state can be assessed by optical metabolic imaging (OMI) (i.e., the analysis of the relative autofluorescence [AF] contributions of the metabolic cofactors NAD(P)H [reduced forms of nicotinamide adenine dinucleotide and nicotinamide adenine dinucleotide phosphate] and flavins [oxidized forms of flavin mononucleotide and flavin adenine

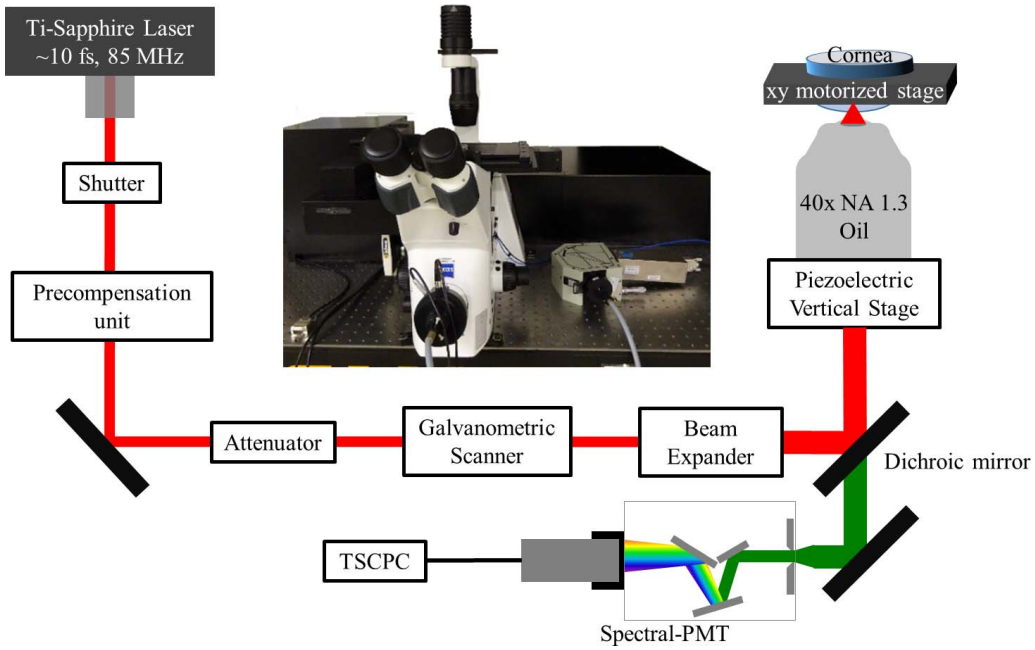

Figure 1. Instrumental setup of the 5D laser-scanning microscope used for AF lifetime and second-harmonic generation imaging of the human cornea. The system has axial, lateral (3D), temporal (4D), and spectral (5D) resolutions of 1 to 2 µm, 0.3 µm, 170 ps, and 12.5 nm, respectively. The pulse width at the cornea was ~12 fs.

dinucleotide]). The AF lifetime, that is, the average time an endogenous fluorophore spends in the excited state, can be used for fluorescence lifetime imaging (FLIM).[6] The fluorescence lifetime depends also on the fluorophores' microenvironment, allowing to discriminate between free and protein-bound configurations, which are in turn affected by the cell metabolism.[8,9] As such, FLIM can be used to infer the cells' metabolic state.[8,10]

The structural organization of the corneal stroma can be assessed using second-harmonic generation (SHG) imaging. SHG is a nonlinear, coherent process generated by interaction of light with structures with noncentrosymmetric molecular organization, such as collagen.[11] Because the stroma is mostly composed of highly organized collagen fibers, SHG is ideal to retrieve information on its architecture.

In this study, spectrally resolved FLIM and SHG imaging were used to characterize both the morphology and metabolic state of human corneas. All layers of the cornea were characterized using SHG and NAD(P)H AF. The AF free to protein-bound ratios were then used to establish correlations between the metabolic activities of epithelial cells, endothelial cells, and keratocytes and the storage time. Alterations to the organization of the corneal stroma fibers during storage were also addressed. We demonstrate that TPI can provide information on the human cornea, not accessible by the current clinical devices, with the potential to improve sample selection prior to transplantation and optimize the storage conditions.

Methods

Preparation of Human Cornea Samples

Human corneas were provided by the Lions Cornea Bank Saar-Lor-Lux, Trier/Westpfalz at the Department of Ophthalmology, Saarland University Medical Center, Homburg/Saar, Germany. Until image acquisition, the corneas were stored in Culture Medium II with Dextran T500 (#F9017; Biochrom GmbH, Berlin, Germany) supplemented with 5% newborn calf serum (#S0415; Biochrom GmbH) at 37°C under a 5% CO_2 atmosphere.

A total of 10 samples was used. Based on storage time, they were divided into three groups:

- Short-term storage (STS): <1 week of storage ($n = 4$)
- Medium-term storage (MTS): between 3 and 4 weeks of storage ($n = 3$)
- Long-term storage (LTS): between 8 and 13 weeks of storage ($n = 3$)

Samples had ECDs of 1733 ± 54 and 1824 ± 53 cells/mm^2 when calculated manually and with the NAVIS cell count system (Nidek Technologies, Erlangen, Germany), respectively. ECDs were determined in the central region of the cornea.

For image acquisition, the samples were washed in PBS and placed in glass-bottom petri dishes. Live-cell imaging solution (#A14291DJ; Life Technologies, Carlsbad, CA, USA) was used to ensure the cornea hydration during imaging. For imaging the endothelium and the Descemet's membrane, the samples were flipped.

All experiments were conducted following the tenets of the World Medical Association Declaration of Helsinki for research using human samples.

FLIM and SHG Imaging

Image acquisition was performed with a custom-built 5-dimensional (5D) laser scanning microscope (JenLab GmbH, Jena, Germany) (Fig. 1). The instrumental setup is described elsewhere.[12] Briefly, it consists of a modified inverted microscope with a galvanometric scanner unit and a piezo-electric stage for z positioning of the objective. An 85-MHz mode-locked titanium-sapphire laser (Integral Pro 400; Femto-Lasers Produktions GmbH, Vienna, Austria) generating ~10-fs pulses with an M-shaped spectral profile (centered at 800 nm) and a bandwidth of ~95 nm was used for sample excitation. The laser pulses were focused onto the sample with a 40× 1.3

NA oil immersion objective (working distance of 210 μm). Signals were detected in reflection geometry, via the same objective, by a 16-channel PMT detector (16PML-PMT; Hamamatsu Photonics, Hamamatsu, Japan) in an overall spectral range between 400 and 600 nm, in combination with a time-correlated single photon counting (TCSPC) SPC-150 module (Becker & Hickl GmbH, Berlin, Germany).

The 5D images were obtained with axial, lateral (3D), temporal (4D), and spectral (5D) resolutions of 1 to 2 μm, 0.3 μm, 170 ps, and 12.5 nm, respectively. The acquisition time for frames with 128 × 128 pixels was 7.4 seconds. Typically, 9 to 13 frames were averaged per image to collect enough photons for an adequate analysis of AF lifetimes. Laser powers between 6 and 15 mW at the sample were used depending on depth position. Intensity images were generated based on the number of photons detected in each pixel. AF lifetime fitting was used to generate the pseudo-colored FLIM images.

Image Analysis

FLIM images were analyzed using the commercial software SPCImage version 5.2 (Becker & Hickl GmbH, Berlin, Germany). The AF decay times were retrieved by fitting the measured decay data, after deconvolution with the instrument response function (IRF), using a two-exponential decay function of the form $F(t) = a_1 e^{-t/\tau_1} + a_2 e^{-t/\tau_2}$, where $F(t)$ is the fluorescence intensity at time t, and a_1 and a_2 are the relative contributions of the fluorescence lifetimes τ_1 and τ_2, respectively. The mean AF lifetime was calculated as $\tau_m = a_1 \tau_1 + a_2 \tau_2$. For a precise analysis of the AF lifetime data, neighboring image pixels were binned to ensure a minimum of ~1000 photon counts per binned area.

The spectral intervals selected for AF and SHG analysis in each layer of the human cornea were chosen based on the spectra of the individual fluorophores in solution.[13] The used spectral ranges are shown in Table 1.

Signals detected between 425 and 500 nm were attributed to NAD(P)H.[13] Theoretically, using the 16-channel PMT detector, the AF signals could be further separated between NAD(P)H and flavins. However, that was not possible due to the very low concentration of flavins in the cornea[14] and the low sensitivity of the spectral PMT detector. Even selective excitation NAD(P)H and flavins at 760 and 850 nm, respectively, revealed only a negligible flavins signal compared with the one of NAD(P)H (data not shown).

The textures of Bowman's layer and stroma SHG images were analyzed using gray-level co-occurrence matrices (GLCMs). This statistical tool computes how often similar pixel pairs specifically spaced occur in an image. Using GLCMs, the correlation between neighboring pixels was analyzed along the vertical, horizontal, and diagonal directions with distances ranging from 1 to 16 μm. The organization of collagen in fiber structures can be inferred on using the decay rate of the correlation with distance. When collagen is organized in fiber structures a fast decrease of the correlation values with distance is expected in all directions, whereas when collagen is randomly organized the correlation should stay constant.[15]

Collagen fibers orientation was analyzed using an algorithm based on Mega et al.[16] First, the images were divided into equally sized areas with 400 × 400 pixels corresponding to an area of 80 × 80 μm^2. The ideal area size was empirically determined. A 2D fast Fourier transform (FFT) was then performed, and subsequently, the low and the high frequencies were reduced by a band pass filter, the contrast was adjusted by shifting the histogram, and the FFT image was smoothed by a median filter. Finally, the radon transform was applied to obtain the frequentness of the different orientation.

Table 1. Detection Ranges Used for Spectral AF Lifetime Analysis of Each Layer of the Human Cornea

Corneal Layer	Detection Range, nm
Epithelium	425–500
Bowman's layer	425–575
Stroma (AF)	425–575
Stroma (SHG)	400–425
Descemet's membrane	425–575
Endothelium	425–500

Let $O \in [0, 180)^{\circ}$ be the set of orientations and let $f(o)$ be the frequentness of the orientation $o \in O$ in the SHG image. Then, $d = \underset{o \in O}{\operatorname{argmax}} f(o)$ is called the dominant orientation and

$$PP = \sqrt{\frac{1}{n-1} \sum_{o \in O} (f(d) - f(o))^2}$$

is the deviation of frequentness of orientations from the dominant orientation, and it is related to the peak prominence of the frequentness function $f(o)$. If the value PP is large, $f(o)$ has a sharp peak at its maximum d, and the fibers are well organized toward the dominant orientation. If, on the other hand, the value PP is small, the peak at the dominant orientation is broad and the fibers are not organized.

The 3D representations of the cornea were created by rendering individual and sequential en face images using the Visualization Toolkit (VTK) within MATLAB (The MathWorks, Inc., Natick, MA, USA).[17]

Statistical Analysis

Statistical analysis was performed using GraphPad Prism version 6.05 (GraphPad Software, Inc., La Jolla, CA, USA). Results are presented as means and SDs. Differences between different storage times were examined using the Mann-Whitney U test. Only P values <0.05 were considered statistically significant.

Results

Corneal Morphology

Figure 2 shows 3D representations of an MTS cornea from the epithelial (Fig. 2A) and endothelial (Fig. 2B) sides reconstructed from a stack of AF intensity (red) and SHG (green) images with 2-μm intervals.

En face AF intensity (red) and SHG (green) images of the same sample are shown in Figure 3. Wing (D ~5 μm and D ~15 μm) and basal cells (D ~30 μm) can be distinguished in the corneal epithelium. Within the cells, the mitochondria distribution is visible. In basal cells, mitochondria are distributed mainly around the cell nuclei. In differentiated cells mitochondria are randomly distributed though the cell cytoplasm (Fig. 3).

At the interface between the epithelium and the Bowman's layer (D ~35 μm), both basal cells AF (red) and collagen SHG (green) from the Bowman's layer were detected. SHG and AF signals originating from the collagen were detected in both the Bowman's layer (D ~45 μm) and the stroma (D ~90 μm). In the corneal stroma, single keratocytes (indicated by the white arrows) are visible.

In the Descemet's membrane (F ~16 μm) a strong AF signal was detected. In the endothelium (F ~2 μm) a regular arrangement of cells as well as a high mitochondrial density were observed.

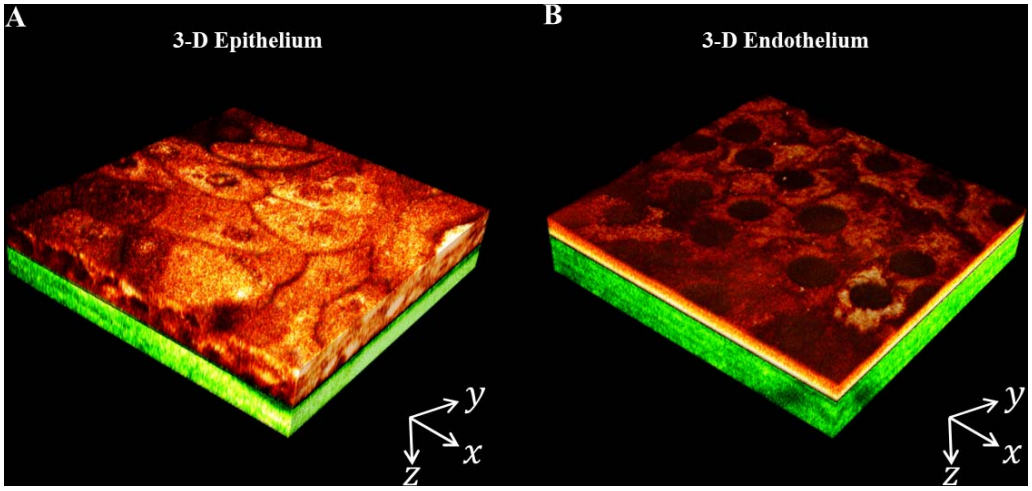

FIGURE 2. 3D representations of the human cornea from the (**A**) epithelial and (**B**) endothelial sides. Volumes were reconstructed from individual and sequential autofluorescence intensity (*red*) and second-harmonic generation (*green*) images recorded with 2-μm intervals along the z axis. The 3D reconstructions represent volumes of approximately 150 × 150 × 150 and 120 × 120 × 50 μm^3 for the epithelial and endothelial sides, respectively.

The thicknesses of the corneal layers, measured by TPI, are shown in Table 2. The epithelial layer was thinner for MTS corneas than for STS corneas, and its thickness decrease further in LTS samples (6 to 15 μm).

Corneal Metabolic State

The cells' metabolic state was assessed using AF lifetimes (τ) and free to protein-bound ratios of the metabolic cofactors. Figure 4 shows representative FLIM images of the epithelium (Fig. 4A), stroma (Fig. 4B), and endothelium (Fig. 4C).

In the corneal stroma, AF stems from collagen and keratocytes (white arrows). Due to the high overlap of the AF spectra of collagen and the metabolic cofactors,[13] a separate analysis of keratocytes AF was only possible by analyzing regions of interest (ROI) with single keratocytes. For MTS corneas, these cells had NAD(P)H mean AF lifetime (τ_m) of 0.56 ± 0.17 ns.

Table 3 shows τ values and relative contributions (a) obtained for each layer of STS human corneas. τ values represent the maximum of the frequency histogram of the image. All cell types composing the epithelial layer were considered. In the epithelium and endothelium, NAD(P)H free to protein-bound ratios were computed by dividing the relative contributions of its free component (a_1) by its protein-bound component (a_2) (Table 3).

Autofluorescence Lifetime Alterations With Sample Storage Time

Figures 5 shows representative images of the NAD(P)H free to protein-bound ratios (a_1/a_2) of epithelial (Fig. 5A) and

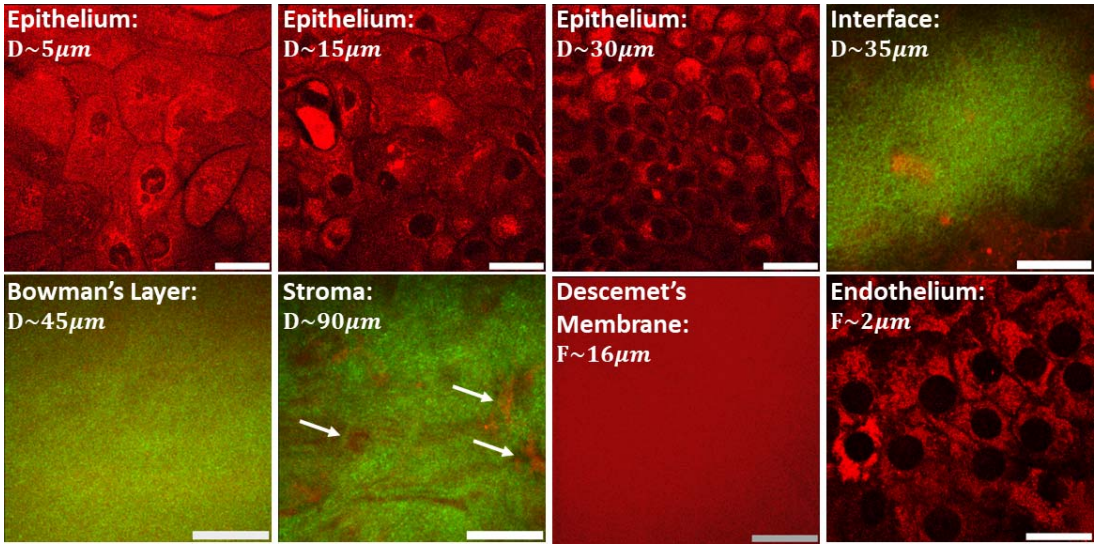

FIGURE 3. En face autofluorescence intensity (*red*) and second-harmonic generation (*green*) images of the human corneal epithelium, Bowman's layer, stroma, Descemet's membrane, and endothelium, as well as the interface between the epithelium and Bowman's layer. Stromal keratocytes are indicated by the *white arrows*. The relative depth position is indicated in each image. The distances D and F are measured relatively from the corneal epithelium and endothelium, respectively. The signal brightness in each pixel represents the number of detected photons. *Scale bars* denote 30 μm.

Investigative Ophthalmology & Visual Science

Table 2. Variation of the Layer Thickness of STS and MTS Human Corneas

Corneas	Epithelium	Bowman's Layer	Descemet's Membrane	Endothelium
STS thickness, μm	40–55	5–10	10–16	6–10
MTS thickness, μm	12–39	6–18	8–11	5–6

Values are presented as measured thickness range (minimum–maximum).

endothelial cells (Fig. 5C) at different storage times. The average variations of NAD(P)H a_1/a_2 in epithelial and endothelial cells with storage time are shown in Figures 5B and 5D, respectively. A significant increase in NAD(P)H a_1/a_2 of corneal epithelial cells was observed for LTS and MTS samples, compared with STS corneas, as well as for LTS corneas compared with MTS corneas (Fig. 5B). In the endothelial cells, NAD(P)H a_1/a_2 was significantly higher in MTS corneas than in STS samples (Fig. 5D).

For keratocytes, NAD(P)H a_1/a_2 was significantly decreased in LTS corneas (1.23 ± 0.20) compared with MTS samples (2.94 ± 0.71).

ECD

TPI AF intensity images of the corneal endothelium (Fig. 6A) were used to retrieve the cells' density, average shape, width, and size. The lack of AF signals from the cell nuclei and cellular membranes (dark areas) enables easy identification of single cells. The contours of individual cells were manually highlighted (Fig. 6B), and segmented for the analysis (Fig. 6C). The endothelial cells of the MTS samples had an average of 7 ± 1 sides with lengths of approximately 39 ± 6.1 μm, making up a total area of approximately 706.3 ± 194.5 μm^2. Based on the number of the cells in the field-of-view (counted using stereologic methods), an ECD of 1461 ± 190 cells/mm^2 was estimated for MTS human corneal samples.

Structural Organization of Collagen Fibers

The collagen in the Bowman's layer and stroma can be observed using SHG imaging. Figure 7 shows SHG images of the Bowman's layer and the anterior stroma at depths of approximately 0, 25, 50, 75, and 100 μm, as well as a 3D representation. As visible in the figure, backward-detected SHG appears as homogenous and speckle-like intensity signals.

The correlations between neighboring pixels as function of distance in the stroma of STS, MTS, and LTS samples, obtained using GLCM, are shown in Figure 7C. For STS samples, a fast decrease of the correlation value is observed in all directions. For MTS and LTS samples, in the same distance range, the decrease in correlation is progressively slower. The correlation value decreases faster with distance for the stroma than for the Bowman's layer (Fig. 7C).

Figure 7D shows the PP value for STS, MTS, and LTS corneas. A consecutive decrease in PP is observed during storage time. PP was significantly lower in MTS and LTS corneas compared with STS samples.

Discussion

Spectrally and spatially resolved FLIM and SHG imaging were used to characterize the status of human corneal samples. Like current clinical methodologies, TPI can be used to assess the morphology of the human cornea. Furthermore, it provides additional information on the cells' metabolism and collagen structural organization.

Using the AF intensity of the metabolic cofactors, it was possible to assess the morphologic characteristics at different depths inside the human cornea with subcellular resolution. The metabolic cofactors are present in the cells' cytoplasm and mitochondria.[18] This allows to recognize single cells, even single mitochondria and the nonfluorescent nucleus, and to discriminate cell layers. The use of TPI AF intensity to investigate the corneal cell morphology was first demonstrated with rabbit's corneas by Piston et al. in 1995.[19] Since then, it has been applied by us and other groups ex vivo to cornea samples of porcine,[20–22] mouse,[23] and human,[24,25] and in the case of rabbits also in vivo.[26]

Here, we could identify different cell types in the human corneal epithelium (Fig. 3C) by the cell morphology. Furthermore, due to the high spatial resolution of TPI, the visualization of mitochondria and their distribution in cells was possible (Figs. 3A–3C).

Layer thickness characterization was also possible using TPI due to its intrinsic optical sectioning. The layer thicknesses measured are in line with the literature.[27] The decrease in epithelial thickness observed in MTS and LTS indicates cell loss

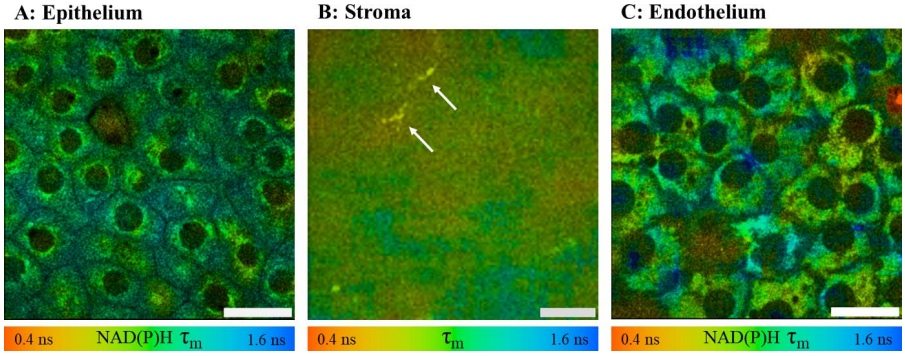

Figure 4. AF lifetime (FLIM) images of the human cornea: (**A**) epithelium; (**B**) stroma; and (**C**) endothelium. Epithelial and endothelial FLIM images are pseudo-color-coded for NAD(P)H mean AF lifetime (detection range: 425 to 500 nm). Stroma FLIM image is pseudo-color-coded for the mean AF lifetime (detection range: 425 to 500 nm: AF of collagen and keratocytes). Stromal keratocytes are indicated by the *white arrows*. AF lifetime ranges are as indicated in the color bar. *Scale bar* denotes 30 μm.

Investigative Ophthalmology & Visual Science

Table 3. AF Lifetimes, Relative Contributions, and Free to Protein-Bound Ratios of STS Human Corneas

AF Lifetime Parameter	Epithelium	Bowman's Layer	Stroma	Descemet's Membrane	Endothelium
τ_1, ns	0.41 ± 0.09	0.37 ± 0.09	0.24 ± 0.07	0.28 ± 0.05	0.31 ± 0.06
τ_2, ns	1.83 ± 0.15	2.07 ± 0.20	2.10 ± 0.10	2.11 ± 0.04	1.76 ± 0.13
τ_m, ns	1.08 ± 0.13	1.27 ± 0.13	1.04 ± 0.20	1.15 ± 0.09	0.97 ± 0.05
a_1, %	52.6 ± 2.7	47.0 ± 5.5	57.0 ± 8.7	52.2 ± 3.2	54.4 ± 1.9
a_2, %	47.4 ± 2.7	53.0 ± 5.5	43.0 ± 8.7	47.8 ± 3.2	45.6 ± 1.9
Ratio a_1/a_2 (free:protein-bound)	1.12 ± 0.12	—	—	—	1.20 ± 0.09

Values are represented as mean ± SD.

with storage. Thus, during this time, the epithelium cannot regenerate the sloughed off cells.

The analysis of the metabolic cofactors AF lifetime by TPI allows to retrieve information on the cells' metabolic state. This has been demonstrated in both animal and human corneas ex vivo.[13,21,28–30] In the human corneal epithelium and endothelium, two lifetime components were observed, consistent with the lifetimes reported for free (τ_1) and protein-bound (τ_2) NAD(P)H (Table 3).[31]

The evaluation of corneal cells metabolism can be an important parameter for assessing the suitability of human corneas for transplantation, particularly for endothelial cells, because they do not regenerate, and a high enough cell density is required for proper function of this layer.[27] The possibility of evaluating corneal metabolic alterations occurring during sample storage was demonstrated for epithelial cells, endothelial cells, and stroma keratocytes. We observed a significant increase in NAD(P)H a_1/a_2 of epithelial and endothelial cells with storage time (Figs. 5A, 5B). An increase of NAD(P)H a_1/a_2 of epithelial cells with storage time was already reported.[29] These results are consistent with an anticipated decrease of the metabolic activity of epithelial and endothelial cells during storage. In contrast, in LTS samples, keratocytes' NAD(P)H a_1/a_2 decreased, indicating that the metabolic activity of keratocytes increases with storage time. Usually in the quiescent state, these cells are activated in case of corneal injury.[27] Such an activation could also take place with storage time.

Characteristics such as the ECD, width, average shape, and area of endothelial cells are usually assessed prior to transplantation. In this study, a manual segmentation of the AF intensity imaged of endothelial cells was performed to assess ECD (Fig. 6). The estimated ECD at the time of the experiments was lower than the one provided with manual count. Likely, the ECD decreased further during the additional storage time. The lengths and shapes of the cells measured were larger than those reported for the healthy endothelium.[27] However, the larger cell lengths and shapes are consistent with cell migration and expansion as a response to endothelial cell loss.[27]

Another important feature of TPI is the feasibility to assess the stromal collagen architecture. Corneal transparency,

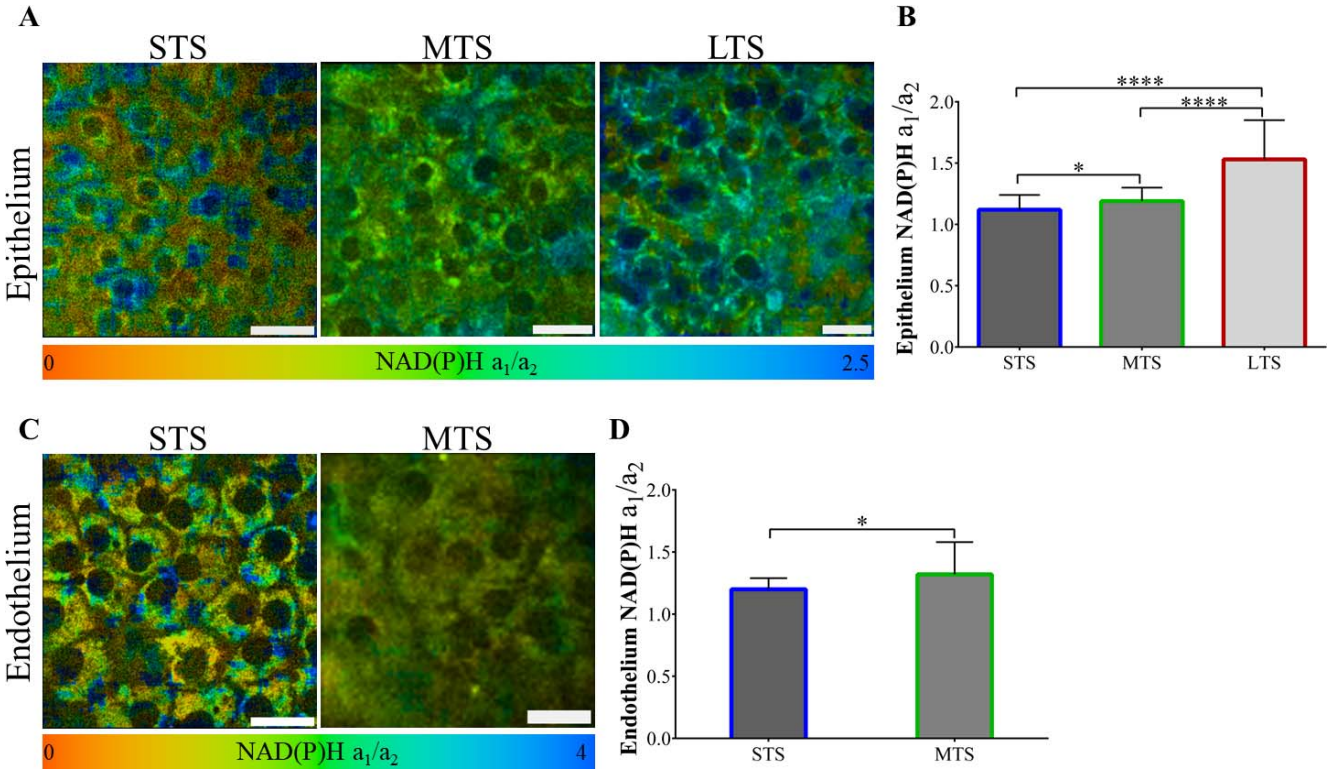

Figure 5. NAD(P)H free to protein-bound (a_1/a_2) ratio alterations with storage time. (**A**) NAD(P)H a_1/a_2 images of the cornea epithelium with STS, MTS, and LTS. (**B**) Average variation of NAD(P)H a_1/a_2 ratio of epithelial cells with storage time. (**C**) Cornea endothelium NAD(P)H a_1/a_2 images of STS and MTS corneas. (**D**) Mean variation of NAD(P)H a_1/a_2 ratio of endothelial cells with storage time. NAD(P)H a_1/a_2 ranges are as indicated in the color bar. *Scale bar* denotes 30 μm. *Statistically significant difference ($P < 0.05$); ****statistically significant difference ($P < 0.0001$).

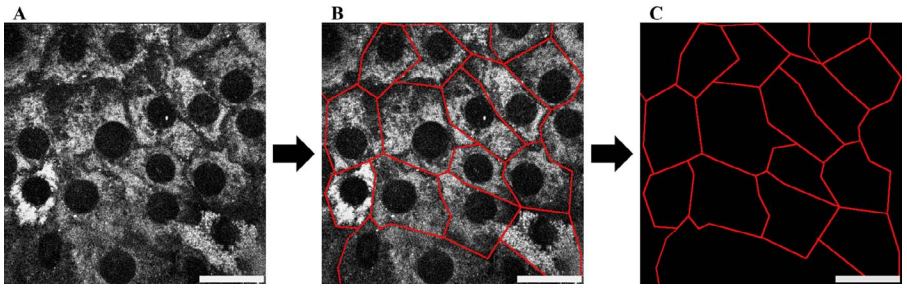

FIGURE 6. Analysis of the ECD in MTS corneal samples using two-photon microscopy. Endothelium (**A**) AF images can be used to assess the cells' morphologic characteristics by (**B**) manually highlighting the cellular contours and thus obtaining the (**C**) segmentation of individual endothelial cells. *Scale bar* denotes 30 μm.

essential for a proper function of the cornea, is intrinsically dependent on the regular arrangement of the stromal collagen fibers.[27] As such, prior to corneal transplantation, the tissue transparency must be also analyzed. With the exception of a few in-house developed systems, this is usually performed subjectively.[32] Using SHG it is possible to assess the structural organization of the collagen fibers.[33–35] Therefore, early alterations of the tissue properties can be detected.

From the Bowman's layer, both SHG and AF signals were detected. Similar to the stroma, this layer is composed of

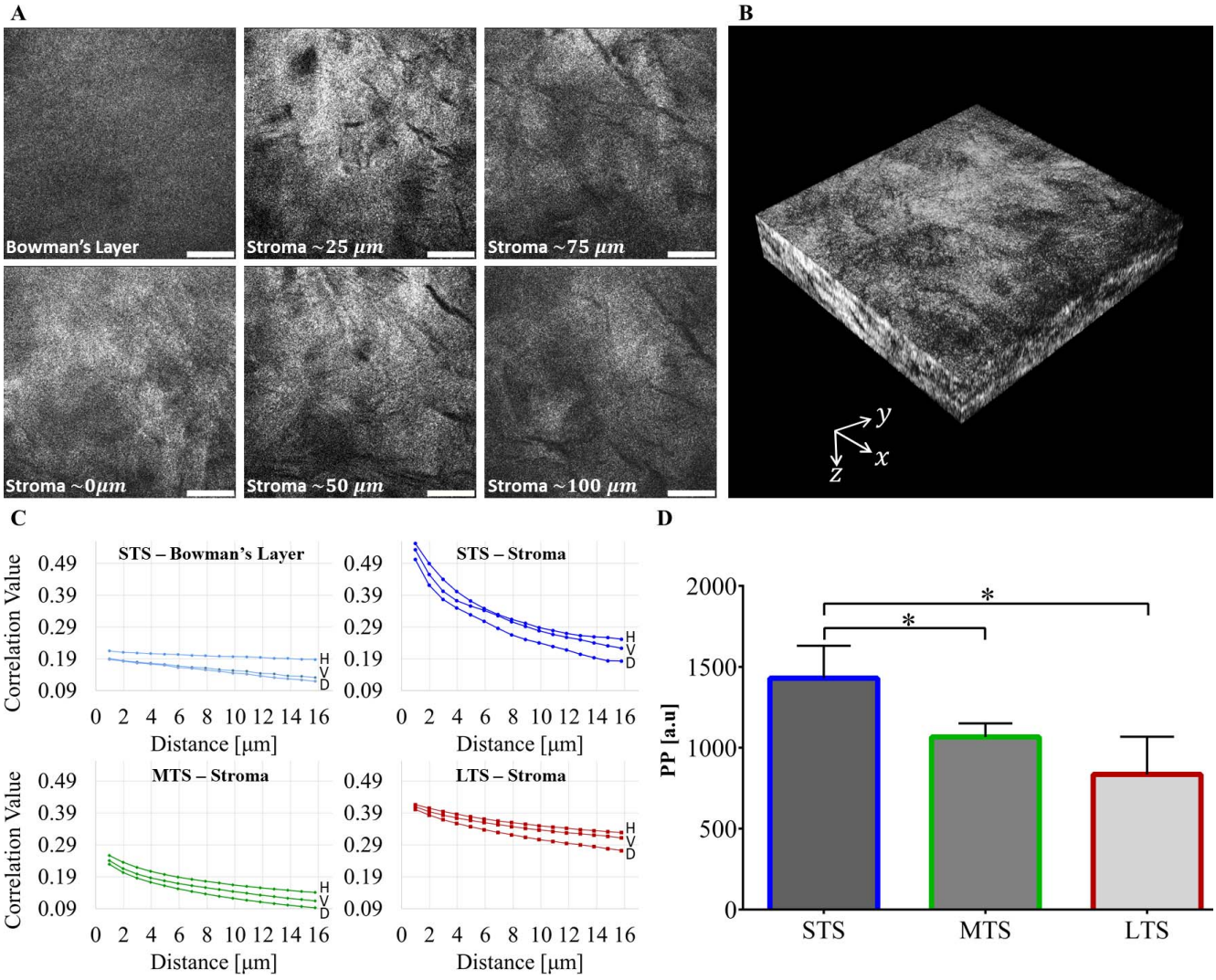

FIGURE 7. Cornea SHG images. (**A**) En face SHG images of the human corneal Bowman's layer and the stroma at depths of 0, 25, 50, 75, and 100 μm. (**B**) 3D reconstruction of approximately $150 \times 150 \times 100$ μm^3 of the stroma reconstructed from individual and sequential SHG images recorded in 5-μm intervals along the z axis. (**C**) Correlation variation as a function of distance in the horizontal (H), vertical (V), and diagonal (D) directions in the stroma of corneal samples with STS, MTS, and LTS, as well as in the Bowman's layer of MTS samples. (**D**) Deviation of frequentness of orientations from the dominant orientation (PP) calculated for the stroma of STS, MTS, and LTS corneas. *Scale bar* denotes 30 μm. *Statistically significant difference ($P < 0.05$).

Investigative Ophthalmology & Visual Science

interwoven collagen fibers.[27] However, a gradual increase in the collagen fibers organization occurs from the Bowman's layer to the stroma and no posterior boundary can be defined.[27] GLCM analysis showed a higher degree of organization into fiber structures of the stroma compared to the Bowman's layer (Fig. 7C).[15]

The analysis of the correlation between neighboring pixels using GLCM also revealed the highest degree of collagen being organized in fiber structures in STS samples, which progressively decreases in MTS and LTS samples, respectively (Fig. 7C).[15]

The orientation and the overall organization of the collagen fibers in the anterior stroma was assessed using an FFT analysis. The collagen fibers' organization was inferred from a PP value (peak prominence). With storage time, a decrease of the PP was observed (Fig. 7D), indicating that the collagen fibers became less oriented toward the dominant orientation, that is, the stroma collagen fibers became less organized.

In the Descemet's membrane, only AF signals were detected. In this layer, the collagen is not organized macroscopically in noncentrosymmetric structures, which are required for SHG generation.[36] The lack of a SHG signal in the Descemet's membrane has already been reported for the porcine[21,37] and human corneas.[24]

Although the main constituent of the Bowman's layer, stroma, and Descemet's membrane is the same (collagen), the collagen types and concentration vary between them. As such, because different collagen types present different lifetimes,[38] these layers of the cornea also have different AF lifetimes (Table 3). Furthermore, the presence of other molecules, such as glycoproteins in the Descemet's membrane, may influence the collagen microenvironment, which will reflect on the AF lifetime. In the stroma, the AF of the keratocytes also contributes to the AF lifetime.

In this study, we demonstrated that TPI can be used to characterize both the morphology and metabolism of human corneas. The alterations due to storage time in the metabolic activity of the epithelium, endothelium, and keratocytes can be assessed. Moreover, changes in the organization of the collagen stroma can be monitored. However, the reduced working distance of the high NA objective used to achieve the highest resolution, limited the analysis of the stroma to the anterior portion, and the samples needed to be flipped for imaging Descemet's membrane and endothelium. We intent to improve the imaging depth of the system to enable the analysis of the entire (anterior, medium, and posterior) stroma organization. In the near future, we will also use clinical two-photon imaging systems (certified multiphoton tomographs), for the optical analysis of donor cornea for transplantation purposes. This may help to better assess the suitability of corneas intended for transplantation and improve the storage conditions, possibly increasing the number of samples suitable for surgery.

Acknowledgments

The authors thank the Lions Cornea Bank Saar-Lor-Lux for providing the human corneas.

Supported by the European Union's Horizon 2020 research and innovation program under Grant 726666 (LASER-HISTO).

Disclosure: **A. Batista**, None; **H.G. Breunig**, None; **A. König**, None; **A. Schindele**, None; **T. Hager**, None; **B. Seitz**, None; **A.M. Morgado**, None; **K. König**, Jenlab GmbH (I)

References

1. Whitcher JP, Srinivasan M, Upadhyay MP. Corneal blindness: a global perspective. *Bull World Heal Organ*. 2001;79:214–221.
2. Crawford AZ, Patel DV, McGhee CN. A brief history of corneal transplantation: from ancient to modern. *Oman J Ophthalmol*. 2013;6(Suppl 1):S12–S17.
3. Gain P, Jullienne R, He Z, et al. Global survey of corneal transplantation and eye banking. *JAMA Ophthalmol*. 2016;134:167–173.
4. Jones GLA, Dekaris I, Hjortdal J, Pels E. European Eye Bank Association: past, present, and future. *Int J Eye Bank*. 2012;1:1–6.
5. Eye Bank Association Of America. *2015 Eye Banking Statistical Report*. Washington, DC: Eye Bank Association of America; 2016.
6. Periasamy A, Clegg RM. *FLIM Microscopy in Biology and Medicine*. Boca Raton, Florida: CRC Press; 2009.
7. Denk W, Strickler J, Webb W. Two-photon laser scanning fluorescence microscopy. *Science*. 1990;248:73–76.
8. Georgakoudi I, Quinn KP. Optical imaging using endogenous contrast to assess metabolic state. *Annu Rev Biomed Eng*. 2012;14:351–367.
9. König K, Schneckenburger H. Laser-induced autofluorescence for medical diagnosis. *J Fluoresc*. 1994;4:17–40.
10. König K, So PT, Mantulin WW, Tromberg BJ, Gratton E. Two-photon excited lifetime imaging of autofluorescence in cells during UVA and NIR photostress. *J Microsc*. 1996;183(Pt 3):197–204.
11. Tian L, Qu J, Guo Z, Jin Y, Meng Y, Deng X. Microscopic second-harmonic generation emission direction in fibrillous collagen type I by quasi-phase-matching theory. *J Appl Phys*. 2010;108:54701–54709.
12. König K, Uchugonova A, Straub M, et al. Sub-100 nm material processing and imaging with a sub-15 femtosecond laser scanning microscope. *J Laser Appl*. 2012;24:42009.
13. Batista A, Breunig HG, Uchugonova A, Morgado AM, König K. Characterization of porcine eyes based on autofluorescence lifetime imaging. *Proc SPIE*. 2015;9329:93290E–8.
14. Batey DW, Eckhert CD. Analysis of flavins in ocular tissues of the rabbit. *Invest Ophthalmol Vis Sci*. 1991;32:1981–1985.
15. Zhuo S, Chen J, Wu G, et al. Quantitatively linking collagen alteration and epithelial tumor progression by second harmonic generation microscopy. *Appl Phys Lett*. 2010;96:94–97.
16. Mega Y, Robitaille M, Zareian R, McLean J, Ruberti J, DiMarzio C. Quantification of lamellar orientation in corneal collagen using second harmonic generation images. *Opt Lett*. 2012;37:3312–3314.
17. Birngruber E, Donner R, Langs G. MatVTK - 3D Visualization for Matlab. In: *Proceedings of the MICCAI 2009 Workshop on Systems and Architectures for CAI*. The Midas Journal; 2009:1–8.
18. Mason WT. *Fluorescent and Luminescent Probes for Biological Activity: A Practical Guide to Technology for Quantitative Real-Time Analysis*. 2nd ed. London, United Kingdom: Elsevier Science; 1999.
19. Piston DW, Masters BR, Webb WW. Three-dimensionally resolved NAD(P)H cellular metabolic redox imaging of the in situ cornea with two-photon excitation laser scanning microscopy. *J Microsc*. 1995;178(Pt 1):20–27.
20. Teng SW, Tan HY, Peng JL, et al. Multiphoton autofluorescence and second-harmonic generation imaging of the ex vivo porcine eye. *Invest Ophthalmol Vis Sci*. 2006;47:1216–1224.
21. Batista A, Breunig HG, Uchugonova A, Morgado AM, König K. Two-photon spectral fluorescence lifetime and second-harmonic generation imaging of the porcine cornea with a 12 femtosecond laser microscope. *J Biomed Opt*. 2016;21:11.
22. König K. High-resolution multiphoton imaging and nanosurgery of the cornea using femtosecond laser pulses. In: Fankhauser F, Kwasniewska S, eds. *Lasers in Ophthalmology:*

Basic, Diagnostic, and Surgical Aspects: A Review. The Haguer, The Netherlands: Kugler Publications; 2003:79–90.

23. Masihzadeh O, Lei TC, Ammar DA, Kahook MY, Gibson EA. A multiphoton microscope platform for imaging the mouse eye. *Mol Vis*. 2012;18:1840–1848.
24. Aptel F, Olivier N, Deniset-Besseau A, et al. Multimodal nonlinear imaging of the human cornea. *Invest Ophthalmol Vis Sci*. 2010;51:2459–2465.
25. König K, Batista A, Breunig HG, Seitz B. Multiphotonen-Tomographie der humanen Kornea. *Ophthalmol Nachrichten Spec Bild*. 2014;09-2014:14–15.
26. König K, Wang B, Krauss O, et al. First in vivo animal studies on intraocular nanosurgery and multiphoton tomography with low-energy 80-MHz near-infrared femtosecond laser pulses. *Proc SPIE*. 2004;5314:262–269.
27. Remington LA. *Clinical Anatomy of the Visual System*. 2nd ed. St. Louis, MO: Elsevier; 2005.
28. Batista A, Breunig HG, Uchugonova A, Seitz B, Morgado AM, König K. Label-free SHG imaging and spectral FLIM of corneas using a sub-15 fs laser microscope. *Proc SPIE*. 2014;8930: 89300V–9.
29. König K, Raphael AP, Lin L, et al. Applications of multiphoton tomographs and femtosecond laser nanoprocessing microscopes in drug delivery research. *Adv Drug Deliv Rev*. 2011; 63:388–404.
30. Batista A, Breunig HG, Donitzky C, König K. Two-photon microscopy and fluorescence lifetime imaging of the cornea. In: König K, ed. *Modern Laser Microscopy and Fluorescence Lifetime Imaging*. 1st ed. Berlin: DeGruyter; 2018:301–320.
31. Schneckenburger H, König K. Fluorescence decay kinetics and imaging of NAD(P)H and flavins as metabolic indicators. *Opt Eng*. 1992;31:1447–1451.
32. Parekh M, Ferrari S, Ruzza A, Pugliese M, Ponzin D, Salvalaio G. A portable device for measuring donor corneal transparency in eye banks. *Cell Tissue Bank*. 2014;15:7–13.
33. Morishige N, Petroll WM, Nishida T, Kenney MC, Jester JV. Noninvasive corneal stromal collagen imaging using two-photon-generated second-harmonic signals. *J Cataract Refract Surg*. 2006;32:1784–1791.
34. Jester JV, Winkler M, Jester EB, Nien C, Chain D, Brown DJ. Evaluating corneal collagen organization using high resolution non linear optical (NLO) macroscopy. *Eye Contact Lens*. 2010;36:260–264.
35. Bueno JM, Gualda EJ, Artal P. Analysis of corneal stroma organization with wavefront optimized nonlinear microscopy. *Cornea*. 2011;30:692–701.
36. Theodossiou TA, Thrasivoulou C, Ekwobi C, Becker DL. Second harmonic generation confocal microscopy of collagen type I from rat tendon cryosections. *Biophys J*. 2006;91: 4665–4677.
37. Jay L, Brocas A, Singh K, Kieffer J-C, Brunette I, Ozaki T. Determination of porcine corneal layers with high spatial resolution by simultaneous second and third harmonic generation microscopy. *Opt Express*. 2008;16:16284.
38. Lutz V, Sattler M, Gallinat S, Wenck H, Poertner R, Fischer F. Characterization of fibrillar collagen types using multi-dimensional multiphoton laser scanning microscopy. *Int J Cosmet Sci*. 2012;34:209–215.

Investigative Ophthalmology & Visual Science